Effects of HIV Protease Inhibitor Ritonavir on Akt-Regulated Cell Proliferation in Breast Cancer

Anjaiah Srirangam[1,6], **Ranjana Mitra**[1,6], **Mu Wang**[2], **J. Christopher Gorski**[1], **Sunil Badve**[3], **Lee Ann Baldridge**[3], **Justin Hamilton**[1], **Hiromitsu Kishimoto**[4], **John Hawes**[9], **Lang Li**[1], **Christie M. Orschell**[1], **Edward F. Srour**[1], **Janice S. Blum**[5,6,7,8], **David Donner**[10], **George W. Sledge**[1,3,6,7,8], **Harikrishna Nakshatri**[2,4,6,7,8], and **David A. Potter**[1,2,6,7,8]

[1]Department of Medicine, Indiana University, Indianapolis, Indiana

[2]Department of Biochemistry and Molecular Biology, Indiana University, Indianapolis, Indiana

[3]Department of Pathology, Indiana University, Indianapolis, Indiana

[4]Department of Surgery, Indiana University, Indianapolis, Indiana

[5]Department of Microbiology and Immunology, Indiana University, Indianapolis, Indiana

[6]Department of Walther Oncology Center, Indiana University, Indianapolis, Indiana

[7]Department of Walther Cancer Institute, Indiana University, Indianapolis, Indiana

[8]Department of Indiana University Cancer Center, Indiana University, Indianapolis, Indiana

[9]Department of Chemistry and Biology, Miami University, Oxford, Ohio

[10]Department of Surgery, University of California, San Francisco, California

Abstract

Purpose—These studies were designed to determine whether ritonavir inhibits breast cancer *in vitro* and *in vitro* and, if so, how.

Experimental Design—Ritonavir effects on breast cancer cell growth were studied in the estrogen receptor (ER)-positive lines MCF7 and T47D and in the ER-negative lines MDA-MB-436 and MDA-MB-231. Effects of ritonavir on Rb-regulated and Akt-mediated cell proliferation were studied. Ritonavir was tested for inhibition of a mammary carcinoma xenograft.

Results—ER-positive estradiol-dependent lines (IC_{50}, 12–24 µmol/L) and ER-negative (IC_{50}, 45 µmol/L) lines exhibit ritonavir sensitivity. Ritonavir depletes ER-α levels notably in ER-positive lines. Ritonavir causes G_1 arrest, depletes cyclin-dependent kinases 2, 4, and 6 and cyclin D_1 but not cyclin E, and depletes phosphorylated Rb and Ser^{473} Akt. Ritonavir induces apoptosis independent of G_1 arrest, inhibiting growth of cells that have passed the G_1 checkpoint. Myristoyl-Akt, but not activated K-Ras, rescues ritonavir inhibition. Ritonavir inhibited a MDA-MB-231 xenograft and intratumoral Akt activity at a clinically attainable serum C_{max} of 22 ± 8 µmol/L. Because heat shock protein 90 (Hsp90) substrates are depleted by ritonavir, ritonavir effects on Hsp90 were tested. Ritonavir binds Hsp90 (K_D, 7.8 µmol/L) and partially inhibits its chaperone function. Ritonavir blocks association of Hsp90 with Akt and, with sustained exposure, notably depletes Hsp90. Stably

Requests for reprints: David A. Potter, Indiana University School of Medicine, 1044 West Walnut Street, R4-202, Indianapolis, IN 46202. Phone: 317-274-3589; Fax: 317-274-0396; E-mail: dapotter@iupui.edu.
Note: A. Srirangam and R. Mitra contributed equally to this work.

expressed Hsp90α short hairpin RNA also depletes Hsp90, inhibiting proliferation and sensitizing breast cancer cells to low ritonavir concentrations.

Conclusions—Ritonavir inhibits breast cancer growth in part by inhibiting Hsp90 substrates, including Akt. Ritonavir may be of interest for breast cancer therapeutics and its efficacy may be increased by sustained exposure or Hsp90 RNA interference.

Recurrent or metastatic breast cancer patients have a median survival of 20 months despite recent advances in chemotherapy (1). The use of sequential single anticancer drugs is an emerging concept in the therapeutics of recurrent or meta-static breast cancer. In this context, novel inhibitors of breast cancer cell growth and survival that differ from existing drugs in their mechanism of action may palliate symptoms and potentially improve survival if they can provide long-term suppression of tumor growth with acceptable toxicity. One candidate inhibitor of breast cancer growth that has not yet been tested in a mammary carcinoma xenograft model is the HIV protease inhibitor ritonavir. Oral bioavailability in humans and a toxicity profile that allows daily dosing are potentially valuable features of ritonavir (2), which may assist in its translation to cancer clinical trials. Ritonavir has been tested in animal models of cancer. Ritonavir blocks the growth of a Kaposi′s sarcoma xenograft in a s.c. tumor model (3) and a syngeneic murine lymphoma model (4) but does not block the growth of glioma (5) or prostate cancer xenografts (6).

The mechanisms by which ritonavir may be involved in cancer inhibition are not well understood. The proteasome has been proposed as a potential nonviral ritonavir target (7), but a recent report indicates that although ritonavir inhibits the 20S proteasome *in vitro* it enhances *in vitro* 26S proteasome activity, suggesting that ritonavir may be a proteasome modulator rather than a direct inhibitor (4). We therefore decided to identify signaling pathways that may be important for the activity of ritonavir, which may lead to better understanding of its activity in breast cancer. Among potential pathways that may be affected by ritonavir, pathways that affect Akt signaling must be considered, because ritonavir can induce apoptosis in glioma lines that are dependent on phosphatidylinositol 3-kinase (PI3K) albeit at concentrations of 100 µmol/L (5). Furthermore, ritonavir inhibits differentiation-associated Akt activity in osteoclasts (8), suggesting that ritonavir may also inhibit Akt phosphorylation in some cancer cells. The estrogen receptor (ER) – negative line breast cancer line, MDA-MB-231, is a line known to be dependent on Akt activity for survival under stress conditions and exhibits high-level constitutive Akt phosphorylation (9). MDA-MB-231 is also protected from paclitaxel- and Fas receptor – induced apoptosis by PI3K/Akt signaling (10,11). The MDA-MB-231 line is also potentially useful for xenograft studies of ritonavir because of its virulent activity in a breast cancer mammary fat pad model (12). Other breast cancer lines that are also protected by Akt from chemotherapy-induced apoptosis include the ER-positive lines MCF7 and T47D (13). The T47D, MCF7, and MDA-MB-231 lines are also dependent on Akt for proliferation (14,15). These observations suggest that the T47D, MCF7, and MDA-MB-231 lines may be informative for the effects of ritonavir on Akt signaling pathways that may regulate breast cancer proliferation and survival. T47D, MCF7, and MDA-MB-231 lines also exhibit wild-type Rb and can be used to study Rb-dependent cell cycle progression. For proliferation and survival studies, the Rb mutant ($Rb^{-/-}$) breast cancer line MDA-MB-436 line was also included to help determine whether cell cycle arrest is associated with Rb status and to determine whether ritonavir affects the proliferation and survival of a $Rb^{-/-}$ line.

Ritonavir is shown here to inhibit proliferation of ER-positive (IC_{50}, 12–24 µmol/L) and ER-negative (IC_{50}, 45 µmol/L) breast cancer lines. ER is down-regulated by ritonavir in the ER-positive, estradiol-dependent lines. A nontransformed ER-positive breast epithelial line, MCF10A, is less sensitive to ritonavir (IC_{50}, 35 µmol/L) than the ER-positive breast cancer lines. Ritonavir caused Rb-associated G_1 arrest, and G_1-arrested MDA-MB-231 cells exhibit reduced clonogenic efficiency primarily in $S + G_2$-M cells. Ritonavir induced apoptosis in all

lines, associated with reduction of Ser[473] phosphorylated Akt. Myristoyl-Akt, but not K-Ras, rescues breast cancer cells from ritonavir inhibition, suggesting that ritonavir has specific and biologically relevant effects on the Akt kinase. Ritonavir inhibited a MDA-MB-231 xenograft at clinically attainable serum levels (C_{max}, 22 ± 8 µmol/L) and inhibited intratumoral Akt activity. Because ritonavir reduced the levels of many heat shock protein 90 (Hsp90) substrate proteins, including ER-α, cyclin-dependent kinases (CDK), cyclin D_1, and mutant p53, ritonavir was tested for Hsp90 binding and inhibition. Ritonavir binds to Hsp90 with micromolar affinity (K_D, 7.8 µmol/L) and partially inhibits its chaperone function. In the MDA-MB-231 line, ritonavir blocks the association of Hsp90 with substrate proteins and reduces Hsp90 levels quantitatively in a time-dependent manner. Stably expressed Hsp90 short hairpin RNA (shRNA) also reduces Hsp90 levels, inhibits cell proliferation, and increases sensitivity to ritonavir-mediated inhibition of proliferation. These results suggest that ritonavir may be of interest for clinical development in breast cancer and that its efficacy may be increased by Hsp90 RNA interference.

Materials and Methods

Antisera

Primary murine monoclonal antibodies included mouse anti-human Hsp90α/β SPA-830 (Stressgen, Victoria, British Columbia, Canada) and D01, a mouse anti-p53 mouse monoclonal antibody recognizing wild-type and mutant p53 (Santa Cruz Biotechnology, Santa Cruz, CA). The primary rabbit polyclonal antisera included anti-bodies to human ER-α (sc-7207; Santa Cruz Biotechnology), Akt (9272; Cell Signaling Technology, Beverly, MA), phosphorylated Akt (pAkt) recognizing phosphorylated Ser[473] (9271; Cell Signaling Technology), Akt phosphosubstrate antibody recognizing the motif (R/K)X(R/K)-XX(pT/pS) (9611; Cell Signaling Technology), extracellular signal-regulated kinase (9102; Cell Signaling Technology), phosphorylated extracellular signal-regulated kinase antibody recognizing phosphorylated Thr[202] and Thr[204] (9101; Cell Signaling Technology), Hsp90α (SPS771; Stressgen), Rb (554136; Becton Dickinson, San Jose, CA), phosphorylated Rb (pRb; 9308; Cell Signaling Technology), CDK2 (sc-163; Santa Cruz Biotechnology), CDK4 (sc-260; Santa Cruz Biotechnology), CDK6 (sc-177; Santa Cruz Biotechnology), cyclin D_1 (sc-718; Santa Cruz Biotechnology), and cyclin E (sc-481; Santa Cruz Biotechnology).

Cell lines

Breast cancer lines MCF7 and T47D were obtained from the American Type Culture Collection (Manassas, VA). The lines MDA-MB-231 and MDA-MB-436 were obtained from the Nakshatri laboratory (Indiana University, Indianapolis, IN). The MCF7 line CA-Akt, which overexpresses pleckstrin homology domain deleted (deleted for amino acids 4–129), constitutively active Akt [m-(Δ4-129)-Akt], and the corresponding pcDNA3 empty vector line have been described previously (16). The MDA-MB-231 lines CA-Akt-231-2 and CA-Akt-231-12 overexpressing m-(Δ4-129)-Akt as well as the vector control lines 231-V1 and 231-V2 were isolated as described above.

Myristoyl-Akt-overexpressing MDA-MB-231 lines were isolated by adenoviral transduction and selection of stably transduced lines. The myristoyl-Akt insert from the pcDNA3 construct published previously (16) was inserted in the polylinker of the pQCXIP retroviral vector (Clontech, BD Biosciences, Mountain View, CA), which bears a puromycin selection marker. The resulting construct was named pQCXIP/Akt. The constructs pQCXIP/Akt and pQCXIP were transfected into a packaging cell line Phoenix-ampho using FuGENE reagent (Roche Diagnostics, Branchburg, NJ), and infectious, replication-incompetent virus was isolated and used to infect MDA-MB-231 cells. Ring cloned colonies were isolated and cultured with puromycin (300 ng/mL) – containing medium.

The Hsp90α shRNA construct was provided by Dr. S-C. Teng (National Taiwan University; ref. 17). The pSUPER (Oligoengine, Seattle, WA)-based expression plasmid was cotransfected with a pcDNA3 vector (Invitrogen, Inc., Carlsbad, CA), and selection was done using G418 conditions as described above. The vector control consisted of the pSUPER empty vector with a neo selection marker. Isolation of individual clones was done as described above. Measurement of Hsp90 protein levels was done by Western blotting. Only one clone, sh11, exhibited reduction of Hsp90 levels of >30 G418 clones isolated.

The human hemagglutinin-tagged K-Ras V12 construct was expressed in the pCGN plasmid and selected with hygromycin (150 µg/mL; ref. 18). Isolation of individual clones was done as above. To confirm the expression of the hemagglutinin tag antibody, an anti-hemagglutinin antibody was used (MMS-101R; 1:5,000 dilution; Covance, Princeton, NJ). A pool of clones confirmed to be overexpressing hemagglutinin-tagged K-Ras V12 was compared with a vector clone pCGN-V1 expressing the empty vector.

Purification of ritonavir

Ritonavir was purchased and purified from commercially available pharmaceutical liquid using high-performance liquid chromatography (19). Purified crystalline ritonavir was also purchased (Moravek, Inc., Brea, CA or Sequoia Research Products, Pangbourne, United Kingdom).

Radioimmunoprecipitation assay buffer lysates and immunoblot methods

Radioimmunoprecipitation assay buffer (RIPA) lysates were made by standard methodology using protease and phosphatase inhibitors (19,20). Immunoblots were probed and quantified by chemiluminescence (Amersham Biosciences/GE Healthcare, Piscataway, NJ) as described previously (19). Equality of protein loading for SDS-PAGE was determined by micro-BCA assay (Bio-Rad Laboratories, Hercules, CA) and uniformity of transfer between lanes was confirmed by Ponceau staining. Experiments were done in triplicate and assayed for protein levels. Normalization to total protein was validated by measurement of glyceraldehyde-3-phosphate dehydrogenase (GAPDH) or β-actin levels by chemiluminescence antibody detection, which were not affected by ritonavir exposure.

3-(4,5-Dimethylthiazol-2-yl)-2,5-diphenyltetrazolium bromide cell proliferation assay

Cell proliferation was measured in 96-well plates by a 3-(4,5-dimethylthiazol-2-yl)-2,5-diphenyltetrazolium bromide (MTT) assay that measures reduction of MTT in 96-well plates (21). The cells were exposed to 5 to 60 µmol/L ritonavir or DMSO vehicle for 48 hours and proliferation was then quantified by MTT assay. Each assay was done with eight measurements for each data point. Experiments were repeated thrice for confirmation.

Measurement of clonogenic efficiency

Clonogenic efficiency of breast cancer lines was measured by exposing cell monolayers to varying concentrations of ritonavir (10–100 µmol/L) or vehicle for 24 hours, with cell density being 20% of confluence at the beginning of treatment. At the end of 24 hours of exposure to ritonavir or vehicle, monolayers were treated with trypsin to make cell suspensions followed by neutralization of the medium and replating of the cells in complete medium (containing 10% FCS), in the absence of drug, at 500 cells per 100-mm plate. The medium was changed every 3 days for 21 days. At the end of the 21-day incubation, colonies were fixed, stained with crystal violet, and counted. The fraction of control colonies was measured for each drug concentration, in triplicate, and the coefficient of variation was, on average, ~10%.

Estrogen responsiveness of the T47D and MCF7 lines

Estrogen responsiveness of the T47D and MCF7 lines was confirmed by measuring the proliferation of these lines in response to a range of 10 to 1,000 pmol/L estradiol in phenol red – free medium supplemented with charcoal-stripped FCS. A total of 4,000 cells were plated per well in 24-well plates, and cells were starved for estrogen for 2 days before stimulation with estradiol. The cells were then incubated for an additional 48 hours in the presence of estradiol, and a MTT assay was done.

Cell cycle analysis

To study the effects of ritonavir on cell cycle progression in the breast cancer lines, cells from dishes that were 30% to 50% confluent were treated with trypsin, washed, and resuspended in complete medium. After plating at 5×10^5 in a 100-mm plate, the cells were grown for 48 hours in complete medium in the presence of the ritonavir or vehicle (DMSO). Adherent and nonadherent cells were included in the profile. Profiling of propidium iodide (PI) incorporation was done by FACScan analysis (Becton Dickinson). Cell cycle distribution was determined using ModFit software (Becton Dickinson). Hoechst dye/pyronin sorting of G_0, G_1, and S + G_2-M populations was done as published (22). For each population, 250 cells were plated in a 100-mm dish. The medium was changed every 3 days for 21 days, and the number of recovered colonies was counted. For each population, the number of colonies of ritonavir-exposed cells recovered at 21 days was normalized to the number of colonies recovered from DMSO-exposed control cells. The MDA-MB-231 line exhibited the clearest separation of G_0, G_1, and S + G_2-M populations with the Hoechst dye/pyronin method and was therefore was chosen for analysis.

Measurement of apoptosis

Apoptotic cells were detected using an Annexin V-FITC/PI apoptosis detection kit (Oncogene, Boston, MA). After plating at 5×10^5 in a 100-mm plate, the cells were grown for 48 hours in complete medium in presence of the ritonavir or vehicle (DMSO). The culture and drug exposure conditions for the apoptosis assays were done across a range of 5 to 60 µmol/L ritonavir. Cells were harvested by trypsin treatment, washed with complete medium to neutralize the trypsin, and stained with PI and Annexin V-FITC. A total of 1×10^4 events were analyzed per assay by FACScan analysis using CellQuest software (Becton Dickinson). Replicate assays were done to confirm the results.

Measurement of serum ritonavir levels

Serum ritonavir C_{max} levels were measured 1 hour following i.p. ritonavir administration. Serum samples were processed by a liquid-liquid extraction technique. The assay was done as published, with minor modifications (23). The lower limit of quantitation was 50 ng/mL. The relative error for accuracy for ritonavir measurement at 0.4, 2.0, and 8.0 µg/mL was <12%. The coefficient of variation for ritonavir measurements was ≤9%.

Ritonavir treatment of MDA-MB-231 mammary fat pad xenografts

Xenograft studies were done following approval by the Institutional Animal Care and Use Committee at Indiana University Purdue University at Indianapolis (study protocol 2549). The mice were female nude mice (nu$^{-/-}$) 6 to 8 weeks old (Harlan, Indianapolis, IN). For xenograft studies, 1×10^6 log-phase MDA-MB-231 tumor cells were injected into the right mammary fat pad using an established method (24,25). Tumor volume was calculated by the well-known formula: volume (mm^3) = (length) (width)^2 / 2. An interval of 3 weeks was required for the average tumor size to reach 20 mm^3, at which point the mice were randomized to receive either vehicle (50 µL Tween 80; $n = 14$) or ritonavir (40 mg/kg in 50 µL Tween 80; $n = 13$) by i.p. injection for 52 days. On day 52, the remaining mice were sacrificed 1 hour following ritonavir

treatment. Tumors were removed and bisected, with half placed in formalin and half frozen in liquid nitrogen, within 5 minutes of animal sacrifice. Modeling of tumor growth was based on the assumption that tumors exhibit an exponential (Gompertzian) growth rate, where i is the subject identifier and t_j is the jth sampling time point, with tumor $size_{ij} = f(t_j) + e_{ij} =$ baseline $\times \exp[\beta(t_j - t_i)] + e_{ij}$, $e_{ij} = N[0, \sigma^2 \times f^2(t_j)]$, where baseline is the first measurement of tumor size. This model was used to determine the P for the difference in tumor growth between experimental and control arms.

Immunohistochemistry for Akt activity

The rabbit primary antibody used to detect Akt kinase activity was 9611 known to recognize phosphorylation of Akt/AGC kinase substrates, including glycogen synthase kinase-3α and -3β (26). Although some AGC kinase substrates may not be direct Akt kinase substrates, many are downstream of the PDK1/Akt pathway (27). A streptavidin-biotin development system (Universal Developer LSAB2; DAKO, Glostrup, Denmark) was used to develop the slides. Hematoxylin counterstain was followed by dehydration and mounting. Peptide competition to confirm specificity of antibody staining was done using the phosphopeptide used to raise antibody 9611 and resulted in complete inhibition of immunohisto-chemical staining in tumors of vehicle- or ritonavir-treated mice at the manufacturer′s suggested dilutions. A secondary antibody staining control without primary antibody was also done and exhibited no staining. To score tumor staining with the Akt kinase phosphosubstrate assay, >80 cells (82–134 cells) were counted per ×40 field and scored as plasma membrane/cytoplasmic or nuclear predominant staining. The fraction of total epithelial cells that exhibited membrane/cytoplasmic staining was determined for each specimen.

Biomolecular interaction analysis of Hsp90 with ritonavir

Interaction of Hsp90 and ritonavir was monitored using a surface plasmon resonance biosensor instrument, Biacore 3000 (Biacore, Inc., Uppsala, Sweden). Hsp90 was covalently linked to the CM5 sensor chip surface via an amine coupling reaction followed by blocking of the reactive group, which resulted in a bound protein signal of 4,000 resonance units. To avoid precipitation of ritonavir, DMSO was added to 1% final concentration, similar to prior studies of the interaction of ritonavir and the HIV protease and serum proteins (28,29). The Bia-evaluation software version 3.2 was used to measure k_{on} and k_{off} using a simple Langmuir 1:1 global fitting model. Binding study experiments were evaluated for data quality by curve fitting, and data sets exhibiting a χ^2 fit value of <3.0 were analyzed. Binding experiments were done in triplicate for ritonavir and 17-allylamino-17-demethoxygeldanamycin (17-AAG).

Assay of Hsp90 chaperone activity

Hsp90 chaperone activity was assayed by measuring luciferase activity following refolding of heat-denatured enzyme. Firefly luciferase (0.26 µmol/L) was thermally inactivated for 5 minutes at 50°C in denaturation buffer [30 mmol/L MOPS-KOH (pH 7.2), 2 mmol/L DTT] containing either Hsp90 (11 µmol/L) or bovine serum albumin (21 µmol/L). Thermally inactivated luciferase was diluted 10-fold into refolding buffer [10 mmol/L MOPS-KOH (pH 7.2), 50 mmol/L KCL, 3 mmol/L Mg(HOAc) 2 mmol/L DTT] containing 50% rabbit reticulocyte lysate, 3 mmol/L ATP, and an ATP-regenerating system. The reaction mixture was incubated for 30 minutes at 30°C. The luciferase activity was measured using Promega (Madison, WI) Bright Glo luciferase luminescence detection system containing luciferin, added following the 30-minute incubation. For each condition, the Hsp90 or bovine serum albumin control was preincubated with ritonavir or vehicle at room temperature for 30 minutes before luciferase denaturation. Assays were done with a SpectraMax Gemini XS 96-well microtiter plate luminometer.

Immunoprecipitation studies

Levels of Hsp90 and substrate proteins Akt and mutant p53 were not affected at 24 hours of ritonavir exposure, although they were diminished at 48 hours. The 24-hour time point of ritonavir exposure therefore offers a condition under which association of Hsp90 and Akt or p53 may be measured by immunoprecipitation. A total of 500 µg protein was used per immunoprecipitation condition. The extract was precleared by addition of protein A+G agarose (sc-2003; Santa Cruz Biotechnology). The extract was subsequently incubated with the anti-Akt antibody, anti-p53 (DO1), or control nonimmune rabbit or mouse IgG. Protein A+G agarose was added, and incubation continued on a rotator overnight at 4°C. The beads were washed, pelleted by low-speed microcentrifugation, resuspended in SDS-PAGE buffer, and subjected to SDS-PAGE and subsequent Western blot transfer. Ponceau staining of the blot confirmed equal recovery of IgG. All immunoprecipitation experiments were done in triplicate with independently grown cell extracts. Blots were not probed for Akt or mutant p53 because these proteins migrate at the same position as immunoglobulin heavy chain. A TrueBlot (eBioscience, San Diego, CA) protocol using antibodies that preferentially detect the native disulfide form of mouse or rabbit IgG did not allow clear detection of Akt or mutant p53 perhaps related to overloading of the gel by the precipitating immunoglobulin at the 50-kDa migration position of heavy chain.

Results

Ritonavir inhibits proliferation and cloning efficiency of breast cancer lines

The sensitivity of human breast cancer lines to ritonavir is unknown. To determine whether ritonavir inhibits the proliferation of the T47D, MCF7, MDA-MB-231, and MDA-MB-436 breast cancer lines, cells were grown in presence of varying concentrations of ritonavir or vehicle for 48 hours and cell number was monitored by MTT assay. Rito-navir exhibits an IC_{50} for proliferation of the T47D, MCF7, MDA-MB-436, and MDA-MB-231 lines of 12, 24, 40, and 45 µmol/L, respectively (Fig. 1*A*). The nontransformed ER-positive human breast epithelial line MCF10A exhibits an IC_{50} of 35 µmol/L. The ER-positive lines tested, T47D and MCF7, exhibit greater sensitivity to ritonavir than the ER-positive MCF10A line.

The ritonavir IC_{50}s for cloning efficiency were determined for 24 hours of ritonavir exposure to determine whether short-term ritonavir treatment decreases cloning efficiency. The cloning efficiency following ritonavir exposure was determined for each line by replating cells in the absence of ritonavir and comparing colony counts obtained with cells exposed to vehicle only. The cloning efficiency IC_{50}s for the T47D and MCF7 lines are 40 and 60 µmol/L ritonavir, respectively. The MDA-MB-436 and MDA-MB-231 lines exhibit cloning efficiency IC_{50}s of 80 µmol/L ritonavir. A similar order of sensitivity to ritonavir was therefore observed for cloning efficiency and proliferation: T47D > MCF7 > MDA-MB-436 and MDA-MB-231. In control studies, there was no measurable effect of ritonavir exposure on adhesion of cells to plastic (data not shown). These studies indicate that 24-hour ritonavir exposure reduces cloning efficiency of breast cancer cells.

Ritonavir exposure decreases ER-α levels in estrogen-responsive lines

Because the ER-positive lines exhibit greater sensitivity to ritonavir than ER-negative lines and exhibit estradiol-dependent proliferation, it was hypothesized that ER-α levels may be reduced by ritonavir. ER-α levels were therefore assayed and estradiol responsiveness was confirmed for the lines. ER-α levels were decreased by 40% for the MCF7 line ($P = 0.008$) and by 50% for the T47D line ($P = 0.002$) following 48 hours of exposure to ritonavir (45 µmol/L; Fig. 1*B*). The MCF7 and T47D lines used in these studies were confirmed to exhibit estradiol-dependent proliferation. Following 2 days of estrogen deprivation, the MCF7 line responded to an estradiol increase from 10 to 1,000 pmol/L, exhibiting a 1.5-fold increase in

growth rate by MTT assay ($P < 0.05$). Following estrogen deprivation, the T47D line responded to a 0 to 1,000 pmol/L increase of estradiol, exhibiting a 2-fold increase in growth rate ($P < 0.05$). The MDA-MB-436 and MDA-MB-231 lines were confirmed by Western blot not to express ER-α and did not exhibit estradiol responsiveness over the same concentration range of estradiol. Because the ER-positive lines used in these studies proliferate in response to estradiol and ER-α is significantly depleted by ritonavir, these results suggest that some of the greater sensitivity of ER-positive lines may be related in part to ritonavir-mediated ER-α depletion.

Ritonavir induces Rb-associated G_1 cell cycle arrest

To determine whether ritonavir inhibits cell cycle progression of breast cancer lines, cells were grown to 50% confluence and cell cycle distribution was compared by PI flow cytometry at 48 hours of ritonavir exposure (30 and 45 µmol/L; Fig. 2*A*; Table 1). At a ritonavir concentration of 45 µmol/L, the Rb$^{+/+}$ lines exhibit an increase in the G_0–G_1 fraction of 30% of total cells for the ER-positive lines and 15% for MDA-MB-231, whereas the Rb$^{-/-}$ line MDA-MB-436 exhibits a 5% increase (Fig. 2*A*; Table 1). At a concentration of 30 µmol/L ritonavir, the MDA-MB-436 line fails to exhibit an increase in the G_0–G_1 fraction, whereas the Rb$^{+/+}$ lines exhibit increases of 5% to 20% (Table 1). Analysis of a range of ritonavir concentrations (5–60 µmol/L) indicated that 15 µmol/L ritonavir is the threshold for cell cycle inhibition of the T47D line, 30 µmol/L for MCF7 and MDA-MB-231 and 45 µmol/L for MDA-MB-436. At 60 µmol/L ritonavir, the increase in G_0–G_1 cells for the MDA-MB-436 line was only 12%, whereas the other lines exhibited increases from 18% to 25%. A small population of subdiploid cells were observed to the left of the G_0–G_1 peak for each line and apoptosis studies were done below.

To determine whether ritonavir-mediated cell cycle inhibition of the Rb$^{+/+}$ breast cancer line MDA-MB-231 occurs at the G_1 checkpoint, a Hoechst dye/pyronin method of live staining, flow cytometry, and cell sorting was used (22). This method allows separation of G_0, G_1, and S + G_2-M cell populations and assay of each population for viability by cloning. Cells were treated with ritonavir (proliferation IC$_{50}$, 45 µmol/L) or DMSO vehicle for 24 hours, subjected to flow cytometry and sorting, and then plated and assayed for cloning efficiency in the presence of vehicle only. Hoechst dye/pyronin flow cytometry studies showed a cell cycle block at the G_1 checkpoint, exhibiting an increase of the G_1 population from 33% to 49%, whereas the S + G_2-M population fell from 16% to 11% (Fig. 2*B*, *top*). These changes in the G_1 and S + G_2-M populations are consistent with a G_1 block. Ritonavir therefore inhibits proliferation of Rb$^{+/+}$ breast cancer lines in part by inhibition at the G_1 checkpoint. Although the concentration of ritonavir used for this flow cytometry experiment is well below the IC$_{50}$ for inhibition of clonogenic efficiency of 80 µmol/L, the clonogenic efficiency of sorted cell cycle subpopulations from this experiment was measured to determine whether there is a ritonavir-sensitive subpopulation of cells that is segregated in the cell cycle. After sorting, cells were plated for clonogenic assay in absence of ritonavir, and at 21 days, there was no reduction in the number of G_0 or G_1 ritonavir-treated cells compared with corresponding vehicle-treated control cells, but the S + G_2-M population exposed to ritonavir was reduced in clonogenic efficiency by 38% relative to control (Fig. 2*B*, *bottom*; $P = 0.00016$). This finding suggests that the cell cycle block at the G_1 checkpoint is not sufficient to induce cell death, but rather cell death is detected primarily in cells that have progressed past the G_1 checkpoint. Of interest, the transient exposure to ritonavir increased the clonogenic efficiency of the G_0 and G_1 populations, where cytotoxicity of ritonavir could be counterbalanced by induction of multidrug resistance (30), for which ritonavir is a substrate (31). Nonetheless, sustained exposure of the sorted cells to ritonavir (45 µmol/L) for 21 days resulted in no viable colonies from the G_0, G_1, or S + G_2-M populations, indicating that under conditions of long-term

exposure the 45 µmol/L ritonavir concentration is highly effective in killing plated cells and preventing any colony formation.

Ritonavir down-regulates CDK2, CDK4, CDK6, and cyclin D_1 and inhibits pRb

Because ritonavir causes a G_1 block of $Rb^{+/+}$ breast cancer cells, whether ritonavir affects proteins known to regulate the G_1 checkpoint was determined. The $Rb^{+/+}$ MDA-MB-231 and the T47D lines were chosen for further study of cell cycle regulatory proteins. Both lines exhibit reduction of CDK2, CDK4, CDK6, cyclin D_1, and pRb following 24 hours of treatment at the ritonavir IC_{50}, which was 45 µmol/L for the MDA-MB-231 line and 15 µmol/L for T47D (Fig. 2*C*; Table 2). Cyclin E, known to require CDK2 phosphorylation on Ser^{384} for its degradation, is not affected by ritonavir (32). pRb was reduced by 70% for both lines, consistent with the effects of ritonavir on cell cycle progression at the G_1 checkpoint in $Rb^{+/+}$ lines. These results suggest that ritonavir inhibits the G_1 checkpoint in $Rb^{+/+}$ lines in part by reduction of pRb. Because CDKs and cyclin D_1 are substrates of Hsp90 and because Hsp90 inhibitors are known to reduce the levels of these specific substrates, the hypothesis that ritonavir may affect Hsp90 function was considered.

Ritonavir induces apoptosis of breast cancer lines

To determine whether ritonavir induces apoptosis, breast cancer lines were exposed to ritonavir (45 µmol/L) for 48 hours, fixed, and assayed for apoptosis by PI/Annexin V flow cytometry (Fig. 3*A–D*). Early apoptotic cells appear in the bottom right quadrant, whereas late apoptotic cells appear in the top right and necrotic cells in the top left. Ritonavir (45 µmol/L) induces early apoptosis in all lines as evidenced by the 3-fold increase of early apoptotic cells in the ER-positive lines and the 30-fold increase of early apoptotic cells in the ER-negative lines (Fig. 3*A–D*; Table 3). The lower fold increase of apoptosis of the ER-positive lines was related to a higher basal level of early apoptosis (3–5%), but the percentage of early apoptotic cells induced by ritonavir (8–19%) was similar for all lines (Fig. 3*A–D*; Table 3). At 60 µmol/L ritonavir, the fraction of early apoptotic cells reaches 15% to 20% for the ER-positive and MDA-MB-436 lines, whereas the MDA-MB-231 line, in contrast, exhibits a much larger increase of early apoptotic cells (60%), which can also be observed by PI profiling, in which this line also exhibits the largest increase in subdiploid fraction and largest decrease in the G_2-M fraction (data not shown). This finding suggests that the MDA-MB-231 G_2-M cells undergo ritonavir-induced cell death and is consistent with the 38% reduction of clonogenic efficiency of MDA-MB-231 cells that have progressed past the G_1 checkpoint (Fig. 2*B*). Although all of the lines exhibit ritonavir-induced apoptosis, apoptosis was not dependent on Rb-related cell cycle arrest, because the $Rb^{-/-}$ MDA-MB-436 line exhibits significant apoptosis under conditions where the cell cycle block is minimal (45 µmol/L). This finding suggests that ritonavir-induced apoptosis is independent of a G_1 block, further supported by a lack of reduction in cloning efficiency of G_1 cells exposed to ritonavir (Fig. 2*B*).

Ritonavir inhibits Ser^{473} pAkt and expression of constitutively active Akt reduces ritonavir sensitivity of breast cancer lines

Because Akt activity inhibits apoptosis in breast cancer lines and mammary epithelium (33–35), it was asked whether ritonavir-induced apoptosis correlates with diminished Ser^{473} phosphorylation of Akt, which is known to correlate with Akt activity. When treated with ritonavir, the T47D, MCF7, MDA-MB-436, and MDA-MB-231 lines exhibit a 40% to 50% reduction of pAkt (Fig. 4*A*; Table 4). It was asked whether ritonavir-mediated decrease of pAkt is related to decreased total Akt, decreased fractional Akt phosphorylation, or both. Total Akt is unchanged by ritonavir in the T47D and MDA-MB-231 lines, whereas pAkt is decreased 40% to 50%. In contrast, total and pAkt are down-regulated by 40% to 45% in the MCF7 and MDA-MB-436 lines (Fig. 4*A*). Two patterns of ritonavir-associated pAkt reduction were

therefore observed in breast cancer lines, reduction of Akt phosphorylation or protein level (Fig. 4*A*; Table 4). In contrast to pAkt, phosphorylated extracellular signal-regulated kinase was not consistently diminished by ritonavir across the lines studied.[11]

To determine whether ritonavir-mediated inhibition of pAkt is important for breast cancer cell growth, it was asked whether activated Akt can specifically overcome ritonavir inhibition of proliferation in lines where pAkt or Akt levels are reduced. Constitutively active myristoyl-Akt was stably expressed in the MDA-MB-231 and MCF7 lines, which exhibit ritonavir-mediated down-regulation of pAkt and Akt level, respectively. Overexpression of constitutively active Akt in MDA-MB-231 cells results in a 30 μmol/L increase of the ritonavir IC_{50} of both lines stably overexpressing Akt compared with the vector control lines ($P < 0.05$; Fig. 4*B*). Stable overexpression of myristoyl-Akt in MCF7 cells (16) also results in a similar increase in ritonavir resistance relative to a vector control line ($P < 0.05$; data not shown). To determine whether myristoyl-Akt-induced resistance to ritonavir is specific, it was asked whether activation of cell growth pathways other than PI3K/Akt, such as K-Ras/Raf-1, may also promote ritonavir resistance. K-Ras V12 is a strong inducer of Raf-1 signaling in COS cells but is less a less effective activator of PI3K/Akt (36). The MDA-MB-231 clones stably expressing K-Ras V12, in contrast to myristoyl-Akt, exhibit very little change in the shape of the ritonavir dose-response curve and do not exhibit a significant increase in ritonavir IC_{50} (Fig. 4*C*). K-Ras V12 overexpression was confirmed by Western blot for the hemagglutinin tag (data not shown). These results suggest that block of the Akt signaling pathway, in contrast to the K-Ras pathway, is of specific importance to breast cancer inhibition by ritonavir.

Ritonavir blocks the growth of MDA-MB-231 mammary fat pad xenografts in part through inhibition of intratumoral Akt kinase activity

Proliferation of the MDA-MB-231 line is dependent on PI3K/Akt pathways (15), whereas the extracellular signal-regulated kinase inhibitor U0126 exhibits little or no inhibition of this line (37), suggesting that the MDA-MB-231 line is a candidate to study for ritonavir-associated Akt inhibition in a xenograft model. To test the effectiveness of ritonavir treatment on MDA-MB-231 xenografts, nude mice were implanted with 1×10^6 tumor cells and the tumors were established for 3 weeks before treatment with ritonavir. Treatment was initiated when the mean tumor size was 20 mm^3 and animals were distributed to vehicle ($n = 14$) and ritonavir ($n = 13$) groups, such that there was an equal total volume of tumors per group. The growth rate of tumors in the vehicle-treated animals exceeded the growth rate of the ritonavir-treated animals by exponential curve fitting based on a Gompertzian model ($P = 0.001$; Fig. 5*A*). Daily ritonavir at tumor inhibitory doses (40 mg/kg/d) or vehicle were well tolerated, as evidenced by stable animal weights that were indistinguishable between the arms of the study (Fig. 5*B*). The ritonavir-treated animals exhibited a tumor growth delay after day 10, and tumor growth remained delayed for the remainder of the experiment, which ended on day 52. The range of ritonavir C_{max} serum levels, measured 1 hour following i.p. dosing at 40 mg/kg/d, was 22 ± 8 μmol/L (mean ± SE; $n = 9$ evaluable mice) at the termination of the experiment on day 52 as determined by high-performance liquid chromatography assay. These results indicate that ritonavir was effective at tumor inhibition at dosing that is well tolerated and correlates with a C_{max} serum concentration within the range attained in patients (38).

To localize Akt kinase activity within xenograft tumors and determine whether intratumoral Akt kinase activity is inhibited by ritonavir, immunohistochemical assay of the tumors was done. Glycogen synthase kinase-3α and -3β and other Akt phosphorylated substrates can be detected by an antibody that recognizes the Akt phosphorylated motif (R/K)X(R/K)XX(T*/S*), the phosphorylated serine/threonine residues of which are marked with asterisks. A

---

[11]R. Mitra and D.A. Potter, unpublished data.

paracortical region exhibited uniform staining for Akt activity in the tumors of vehicle-treated mice (Fig. 5*C*, peptide competition control, Fig. 5*D*), which was greatly diminished in the tumors of ritonavir-treated mice (Fig. 5*E*, peptide competition control, Fig. 5*F*). Two distinct staining patterns of intratumoral Akt activity were observed, plasma membrane/cytoplasmic predominant staining in the tumors of vehicle-treated mice (Fig. 5*C*) and nuclear predominant staining in the tumors of ritonavir-treated mice (Fig. 5*E*). The nuclear staining in the ritonavir-treated cells was red/brown, speckled, and distinct from the underlying hematoxylin counterstain of the nuclei (Fig. 5*D* and *F*). The fraction of tumor cells exhibiting membrane/cytoplasmic staining (membrane/cytoplasmic / [membrane/cytoplasmic + nuclear]) was 0.84 ± 0.080 for the vehicle-treated tumors ($n = 8$) and 0.20 ± 0.063 for the ritonavir-treated animals ($n = 7$; mean ± SE; $P < 0.0001$, Student's t test). Inhibition of membrane/cytoplasmic staining of Akt phosphorylation products in the tumors of ritonavir-treated animals therefore correlated with inhibition of tumor growth. Peptide competition control studies using the phosphopeptide used to raise the antibody detecting Akt phosphorylation products exhibited complete inhibition of staining of the tumors (Fig. 5*D* and *F*). Of note, the hematoxylin counterstain of the tumors revealed that there was a greater frequency of condensed and fragmented nuclei in the tumors of ritonavir-treated mice (Fig. 5*D* and *F*).

Ritonavir binds to Hsp90 with micromolar affinity and partially inhibits chaperone activity

Because CDKs, cyclin D_1, and Akt are substrates of Hsp90 (39,40) and ansamycin inhibitors of Hsp90, such as 17-AAG, induce G_1 arrest in cancer cells, it was asked whether ritonavir interacts with Hsp90. To determine whether ritonavir binds directly to Hsp90, purified human Hsp90 was attached to a Biacore CM5 sensor chip surface and interaction of immobilized Hsp90 and ritonavir was monitored using a surface plasmon resonance (Fig. 6*A*). A Langmuir 1:1 global fitting model revealed a k_{on} of 2.2×10^3 mol/L^{-1} s^{-1}, k_{off} of 1.7×10^{-2} s^{-1}, and $K_D = k_{off}/k_{on}$ of 7.8 µmol/L. The Hsp90 inhibitor, 17-AAG, was also used as a positive control to confirm that the Hsp90 on the CM5 chip bound a known ligand drug with expected affinity (Fig. 6*B*). Binding of 17-AAG to the same Hsp90 chip revealed a k_{on} of 8.4×10^3 mol/L^{-1} s^{-1}, k_{off} of 5×10^{-3} s^{-1}, and $K_D = k_{off}/k_{on}$ of 0.62 µmol/L, in agreement with published results obtained by other methods (41). Together, these results indicate that ritonavir binds to Hsp90 with a K_D of 7.8 µmol/L, which is 10-fold lower in affinity than 17-AAG but well within a clinically attainable concentration range.

To determine whether ritonavir inhibits Hsp90 chaperone activity, ritonavir was tested for inhibition of luciferase refolding (Fig. 6*C*). The refolding efficiency of ritonavir was 30% in the positive control, which was dependent on the addition of Hsp90 and ATP. The polyketide inhibitor of Hsp90, 17-AAG, also inhibited refolding. Ritonavir at 45 and 100 µmol/L concentration inhibited refolding by 33% and 50%, respectively ($P < 0.05$), with zero inhibition defined as the Hsp90 plus DMSO vehicle control and 100% inhibition being defined as the Hsp90 plus 17-AAG (100 µmol/L) control. Together, these results indicate that ritonavir binds to Hsp90 with micromolar affinity and partially inhibits Hsp90 chaper-one activity.

Ritonavir inhibits interaction of Hsp90 and substrate proteins, including Akt and mutant p53

Because Hsp90 forms a complex with Akt that is necessary for correct folding of Akt and its phosphorylation (40), we investigated whether ritonavir inhibits interaction between Hsp90 and Akt or other Hsp90 substrate proteins, such as mutant p53. Hsp90, Akt, and mutant p53 levels in the MDA-MB-231 line are not affected by 24 hours of ritonavir exposure, allowing assay of interactions between Hsp90 and these substrates at 24 hours (Fig. 6*D*). Equal protein from ritonavir-treated cells and vehicle-treated cells was used as the input for the quantitative immunoprecipitation experiments and equal total protein was recovered as assayed by Ponceau staining of the transferred filters. The blot could not be probed for Akt or p53 because of close migration of the target proteins with the large immunoglobulin heavy chain band, which

migrates at 50 kDa. The amount of Hsp90 immunoprecipitated from the extracts of ritonavir-treated cells by an anti-Akt antibody, assayed in Fig. 6*D*, was reduced by 50% compared with control. The amount of Hsp90 immuno-precipitated from the extracts of ritonavir-treated cells by an anti-p53 antibody recognizing mutant p53 was reduced by 60% compared with control (Fig. 6*D*). Immunoprecipitation with nonimmune rabbit and mouse IgG did not pull-down Hsp90, which served as controls for the anti-Akt and anti-p53 antibodies, respectively (Fig. 6*D*).

Sustained ritonavir treatment depletes Hsp90 and mutant p53 but not Akt expression in the MDA-MB-231 line

Because Hsp90 inhibitors are expected to deplete Hsp90 substrates, it was therefore asked whether sustained exposure to ritonavir depletes substrates Akt and mutant p53. Unexpectedly, even at 48 hours of ritonavir exposure (45 µmol/L), Akt levels are not affected in the MDA-MB-231 line (Fig. 6*E*), consistent with the results at 24 hours (Table 4). This finding suggests that displacement of Akt from Hsp90 in the MDA-MB-231 line does not necessarily result in its depletion, although phosphorylation is inhibited. In contrast, the MCF7 and MDA-MB-436 lines exhibit depletion of Akt (Table 4), indicating that depletion of Akt by ritonavir is line specific. Mutant p53 levels are depleted by 25% ($P = 0.015$) in the MDA-MB-231 line at 48 hours of ritonavir exposure (Fig. 6*E*). Unexpectedly, sustained exposure of the MDA-MB-231 line to ritonavir depletes Hsp90 by 50% ($P = 0.012$) at 48 hours (Fig. 6*E*), which could represent an additional mechanism by which ritonavir could promote inhibition of cell proliferation. Stable Akt levels in the face of depletion of Hsp90 and some of its substrates in the MDA-MB-231 line suggest that ritonavir may stabilize some substrates while depleting others.

shRNA reduction of Hsp90 leads to increased sensitivity of the MDA-MB-231 line to ritonavir

To determine whether sustained quantitative reduction of Hsp90 levels inhibits the growth of the MDA-MB-231 line and increases sensitivity to ritonavir, as predicted by the above results, stably transfected clones expressing Hsp90α shRNA were isolated as described previously (17). Of >30 shRNA-expressing MDA-MB-231 clones isolated and screened for reduction of basal Hsp90α levels, only one clone, sh11, exhibited a reduced Hsp90 level, which is 86% of the V8 vector control level ($P = 0.0022$). The sh11 line exhibited a 50% reduction in growth rate relative to the V8 control line (Fig. 6*F*), showing that even modest reduction of basal Hsp90 levels results in significant inhibition of proliferation.

The sensitivity of proliferation of the MDA-MB-231 line to Hsp90 reduction predicts that the sh11 line expressing Hsp90 shRNA should be more sensitive to ritonavir inhibition than the V8 control line. Exposure of the sh11 line to ritonavir for 48 hours, a time point when Hsp90 levels are reduced by ritonavir, results in a significant shift of the dose-response curve to the left, at ritonavir doses below the IC_{50}. This finding indicates that RNA interference of Hsp90 significantly increases sensitivity of the MDA-MB-231 line to low-dose ritonavir (Fig. 6*G*). At 10 to 40 µmol/L ritonavir concentrations, there are 7- to 1.3-fold increases in inhibition of the MDA-MB-231 line relative to the V8 vector control. The convergence of the ritonavir inhibition curves for the V8 and sh11 lines as the IC_{50} is approached suggests that ritonavir and Hsp90 shRNA are inhibiting a similar target, consistent with the reduction of Hsp90 by both modalities and weaker depletion of Hsp90 by shRNA.

Discussion

Here, ritonavir exhibits single-agent activity against breast cancer lines *in vitro* and *in vitro* at clinically attainable concentrations (38). Ritonavir induces G_1 arrest in $Rb^{+/+}$ lines but does not result in loss of clonogenic efficiency of G_1-arrested cells but rather inhibits cells that have progressed beyond the G_1 checkpoint. Ritonavir depletes cell cycle regulatory proteins known

to be Hsp90 associated, including cyclin D_1 (42), CDK2 (43), CDK4 (44,45), and CDK6 (46), providing a mechanism for G_1 arrest that is related to inhibition of Rb phosphorylation. Ritonavir has no effect on cyclin E, which is dependent on CDK2 for its phosphorylation on Ser^{384} and its turnover by the Fbw7 pathway (32). Ritonavir also depletes pAkt, which has been implicated in bypass of cytokine-mediated G_1 arrest in breast cancer (47,48). Ritonavir induces cell death in all breast cancer lines studied regardless of Rb status and independent of cell cycle arrest. Therefore, the inhibition of proliferation by ritonavir is related in part to G_1 arrest, which does not cause cell death, and in part to death of cells that have passed the G_1 checkpoint. Overexpression of constitutively active Akt promotes resistance to ritonavir inhibition of proliferation and may do so in part by overcoming a G_1 block and in part by inhibiting apoptosis. Whether the rescue effect of Akt is related to cell cycle modulation or resistance to apoptosis will be addressed in future studies. In contrast, activated K-Ras, which activates Raf-1 more than Akt in cultured cells (36), does not overcome ritonavir inhibition of the MDA-MB-231 line, suggesting that ritonavir-mediated inhibition of proliferation is related to inhibition of the PI3K/Akt pathway in contrast to the Raf-1 pathway.

Ritonavir inhibits the MDA-MB-231 xenograft at serum drug concentrations that are clinically attainable (38), suggesting that ritonavir may be translated to early-stage clinical trials for recurrent or metastatic breast cancer. The activity of ritonavir against the MDA-MB-231 xenograft at concentrations below the IC_{50} could be related to depletion of Hsp90. Sustained ritonavir exposure of MDA-MB-231 cells with daily dosing of ritonavir may deplete Hsp90 and increase sensitivity to ritonavir at concentrations of 10 to 30 µmol/L as observed for Hsp90 reduction by shRNA. Consistent with the observed inhibition of Akt phosphorylation by ritonavir in the MDA-MB-231 line, the known dependence of this line on Akt phosphorylation for survival (10,11,49,50), and the specific role of myristoyl-Akt in promoting resistance of this line to ritonavir inhibition of proliferation, ritonavir inhibited Akt activity intratumorally. Depletion of membrane/cytoplasmic Akt activity is consistent with current models of Akt activation at the plasma membrane by PI3K pathways (51–53). Based on the observed inhibition of intratumoral Akt activity by ritonavir, it is possible that immunohistochemical monitoring of intratumoral Akt activity could serve as a pharmacodynamic marker for anticancer activity of ritonavir.

ER-positive lines T47D and MCF7 exhibit the greatest sensitivity to ritonavir. Ritonavir depletes ER-α in ER-positive, estrogen-dependent breast cancer lines, correlating with increased sensitivity of these lines to ritonavir. The ER-positive breast cancer lines are more sensitive to ritonavir than a nontransformed ER-positive breast epithelial line, showing selective inhibition. The inhibition of ER-α is of biological importance, because ritonavir inhibits ER element–driven transcription.[12] Whether Hsp90 inhibition by ritonavir results in reduced ER-α levels will be addressed in future studies. ER also induces multidrug resistance expression more efficiently in the MCF7 line than in T47D, which could explain the higher sensitivity of the T47D line to ritonavir, a multidrug resistance substrate (54).

Ritonavir binds to Hsp90 with micromolar affinity (K_D = 7.8 µmol/L) and partially inhibits its chaperone function. Although the affinity of 17-AAG for Hsp90 is 10-fold higher than ritonavir in these studies, serum ritonavir concentrations attained clinically are in excess of its measured K_D (38). Ritonavir-mediated inhibition of Hsp90 is likely to be important qualitatively through inhibition of chaperone activity and quantitatively by reducing Hsp90 levels. Both effects are likely to be important for its inhibition proliferation of the MDA-MB-231 line, because this line is sensitive to modest reductions of Hsp90. The ability of RNA interference to increase the sensitivity of breast cancer cells to ritonavir at low ritonavir concentrations suggests that

---

[12]E. Vieth, A. Srirangam, M-H. Jeng, and D.A. Potter, unpublished data.

RNA interference or antisense strategies that target Hsp90 could be potentially clinically useful in conjunction with ritonavir.

As a novel Hsp90-binding drug, ritonavir exhibits certain striking similarities to geldanamycin and other Hsp90 inhibitors, such as radicicol. On one hand, depletion of Hsp90 substrates, including ER, CDK2, CDK4, CDK6, and cyclin D_1, is characteristic of this class of drugs; on the other hand, depletion of Akt is cell line dependent. In the MDA-MB-231 line, although complexes of Akt and Hsp90 are disrupted by ritonavir, there is no loss of Akt with time. Because caspase-3, a known Akt protease, is active under these conditions,[11] the observed stability Akt in the MDA-MB-231 line may be due to lack of direction of this substrate to the ubiquitin/proteasome system, which is also known to proteolyze Akt (40). Interestingly, the stable Akt in ritonavir-treated MDA-MB-231 cells is dephosphorylated and therefore likely to be inactive. Because Akt is known to exist in a complex with Hsp90 and these complexes are known to exhibit antiapoptotic activity through phosphorylation and inactivation of the proapoptotic kinase ASK1 (55), it is possible that the disruption of Akt/Hsp90 complexes and dephosphorylation of Akt are more important for ritonavir-induced apoptosis than depletion of Akt. Another apparent difference between ritonavir and geldanamycin and radicicol (56) is that ritonavir significantly depletes Hsp90 levels with sustained exposure. Depletion of Hsp90 by ritonavir may increase the susceptibility of breast cancer cells to cell death by removing a buffer for deleterious mutations that may accumulate in cancer cells (57). This hypothesis may also explain the apparent sensitivity of the MDA-MB-231 line to even modest reduction of Hsp90 levels and could also provide a further explanation for the broad sensitivity of breast cancer lines to ritonavir.

Tumor regrowth between chemotherapy treatment cycles has been proposed to be a fundamental problem that limits the control of recurrent/metastatic cancer, predicted by the Norton-Simon hypothesis (58–60). For this reason, nonmyelosuppressive drugs, such as ritonavir, which may be given daily over months to years and could potentially arrest tumor regrowth, are much needed. The studies presented here indicate that ritonavir may be such a candidate drug, pointing to its potential translation to clinical trials. Akt activity measurement by immunohistochemistry may be a useful biomarker to aid in the clinical development of ritonavir. Combination of ritonavir with RNA interference or antisense approaches that down-regulate Hsp90 may increase the sensitivity of breast cancer cells to low doses of ritonavir and may be of value for clinical development.

Acknowledgments

References

1. Sledge GW, Neuberg D, Bernardo P, et al. Phase III trial of doxorubicin, paclitaxel, and the combination of doxorubicin and paclitaxel as front-line chemotherapy for metastatic breast cancer: an intergroup trial (E1193). J Clin Oncol 2003;21:588–592. [PubMed: 12586793]

2. Kempf DJ, Marsh KC, Denissen JF, et al. ABT-538 is a potent inhibitor of human immunodeficiency virus protease and has high oral bioavailability in humans. Proc Natl Acad Sci U S A 1995;92:2484–2488. [PubMed: 7708670]

3. Pati S, Pelser CB, Dufraine J, Bryant JL, Reitz MS Jr. Weichold FF. Antitumorigenic effects of HIV protease inhibitor ritonavir: inhibition of Kaposi sarcoma. Blood 2002;99:3771–3779. [PubMed: 11986235]

4. Gaedicke S, Firat-Geier E, Constantiniu O, et al. Anti-tumor effect of the human immunodeficiency virus protease inhibitor ritonavir: induction of tumor-cell apoptosis associated with perturbation of proteasomal proteolysis. Cancer Res 2002;62:6901–6908. [PubMed: 12460905]

5. Laurent N, de Bouard S, Guillamo JS, et al. Effects of the proteasome inhibitor ritonavir on glioma growth *in vitro* and *in vivo*. Mol Cancer Ther 2004;3:129–136. [PubMed: 14985453]

6. Ikezoe T, Hisatake Y, Takeuchi T, et al. HIV-1 protease inhibitor, ritonavir: a potent inhibitor of CYP3A4, enhanced the anticancer effects of docetaxel in androgen-independent prostate cancer cells *in vitro* and *in vivo*. Cancer Res 2004;64:7426–7431. [PubMed: 15492266]

7. Andre P, Groettrup M, Klenerman P, et al. An inhibitor of HIV-1 protease modulates proteasome activity, antigen presentation, and T cell responses. Proc Natl Acad Sci U S A 1998;95:13120–13124. [PubMed: 9789051]

8. Wang MW, Wei S, Faccio R, et al. The HIV protease inhibitor ritonavir blocks osteoclastogenesis and function by impairing RANKL-induced signaling. J Clin Invest 2004;114:206–213. [PubMed: 15254587]

9. Dunn SE, Torres JV, Oh JS, Cykert DM, Barrett JC. Up-regulation of urokinase-type plasminogen activator by insulin-like growth factor-I depends upon phosphatidylinositol-3 kinase and mitogen-activated protein kinase kinase. Cancer Res 2001;61:1367–1374. [PubMed: 11245436]

10. Aoudjit F, Vuori K. Integrin signaling inhibits paclitaxel-induced apoptosis in breast cancer cells. Oncogene 2001;20:4995–5004. [PubMed: 11526484]

11. Gibson EM, Henson ES, Haney N, Villanueva J, Gibson SB. Epidermal growth factor protects epithelial-derived cells from tumor necrosis factor-related apoptosis-inducing ligand-induced apoptosis by inhibiting cytochrome *c* release. Cancer Res 2002;62:488–496. [PubMed: 11809700]

12. Zugmaier G, Paik S, Wilding G, et al. Transforming growth factor β1 induces cachexia and systemic fibrosis without an antitumor effect in nude mice. Cancer Res 1991;51:3590–3594. [PubMed: 2054795]

13. Gibson S, Tu S, Oyer R, Anderson SM, Johnson GL. Epidermal growth factor protects epithelial cells against Fas-induced apoptosis Requirement for Akt activation. J Biol Chem 1999;274:17612–17618. [PubMed: 10364198]

14. Acosta JJ, Munoz RM, Gonzalez L, et al. Src mediates prolactin-dependent proliferation of T47D and MCF7 cells via the activation of focal adhesion kinase/Erk1/2 and phosphatidylinositol 3-kinase pathways. Mol Endocrinol 2003;17:2268–2282. [PubMed: 12907754]

15. Fujita N, Sato S, Katayama K, Tsuruo T. Akt-dependent phosphorylation of p27Kip1 promotes binding to 14-3-3 and cytoplasmic localization. J Biol Chem 2002;277:28706–28713. [PubMed: 12042314]

16. Campbell RA, Bhat-Nakshatri P, Patel NM, Constantinidou D, Ali S, Nakshatri H. Phosphatidylinositol 3-kinase/AKT-mediated activation of estrogen receptor α: a new model for anti-estrogen resistance. J Biol Chem 2001;276:9817–9824. [PubMed: 11139588]

17. Teng SC, Chen YY, Su YN, et al. Direct activation of HSP90A transcription by c-Myc contributes to c-Myc-induced transformation. J Biol Chem 2004;279:14649–14655. [PubMed: 14724288]

18. Cox AD, Solski PA, Jordan JD, Der CJ. Analysis of Ras protein expression in mammalian cells. Methods Enzymol 1995;255:195–220. [PubMed: 8524103]

19. Potter DA, Srirangam A, Fiacco KA, et al. Calpain regulates enterocyte brush border actin assembly and pathogenic *Escherichia coli*-mediated effacement. J Biol Chem 2003;278:30403–30412. [PubMed: 12764139]

20. Bhat-Nakshatri P, Sweeney CJ, Nakshatri H. Identification of signal transduction pathways involved in constitutive NF-κB activation in breast cancer cells. Oncogene 2002;21:2066–2078. [PubMed: 11960379]

21. Ohno M, Abe T. Rapid colorimetric assay for the quantification of leukemia inhibitory factor (LIF) and interleukin-6 (IL-6). J Immunol Methods 1991;145:199–203. [PubMed: 1765652]

22. Ladd AC, Pyatt R, Gothot A, et al. Orderly process of sequential cytokine stimulation is required for activation and maximal proliferation of primitive human bone marrow CD34$^+$ hematopoietic progenitor cells residing in G$_0$. Blood 1997;90:658–668. [PubMed: 9226166]

23. van Heeswijk RP, Hoetelmans RM, Harms R, et al. Simultaneous quantitative determination of the HIV protease inhibitors amprenavir, indinavir, nelfinavir, ritonavir and saquinavir in human plasma by ion-pair high-performance liquid chromatography with ultraviolet detection. J Chromatogr B Biomed Sci Appl 1998;719:159–168. [PubMed: 9869376]

24. Cornetta K, Moore A, Johannessohn M, Sledge GW. Clonal dominance detected in metastases but not primary tumors of retrovirally marked human breast carcinoma injected into nude mice. Clin Exp Metastasis 1994;12:3–12. [PubMed: 8287617]

25. Helbig G, Christopherson KW II, Bhat-Nakshatri P, et al. NF-κB promotes breast cancer cell migration and metastasis by inducing the expression of the chemokine receptor CXCR4. J Biol Chem 2003;278:21631–21638. [PubMed: 12690099]

26. Fresno Vara JA, Casado E, de Castro J, Cejas P, Belda-Iniesta C, Gonzalez-Baron M. PI3K/Akt signaling pathway and cancer. Cancer Treat Rev 2004;30:193–204. [PubMed: 15023437]

27. Mora A, Komander D, van Aalten DM, Alessi DR. PDK1, the master regulator of AGC kinase signal transduction. Semin Cell Dev Biol 2004;15:161–170. [PubMed: 15209375]

28. Frostell-Karlsson A, Remaeus A, Roos H, et al. Biosensor analysis of the interaction between immobilized human serum albumin and drug compounds for prediction of human serum albumin binding levels. J Med Chem 2000;43:1986–1992. [PubMed: 10821711]

29. Markgren PO, Lindgren MT, Gertow K, Karlsson R, Hamalainen M, Danielson UH. Determination of interaction kinetic constants for HIV-1 protease inhibitors using optical biosensor technology. Anal Biochem 2001;291:207–218. [PubMed: 11401294]

30. Chandler B, Almond L, Ford J, et al. The effects of protease inhibitors and nonnucleoside reverse transcriptase inhibitors on P-glycoprotein expression in peripheral blood mononuclear cells *in vitro*. J Acquir Immune Defic Syndr 2003;33:551–556. [PubMed: 12902797]

31. Lee CG, Gottesman MM, Cardarelli CO, et al. HIV-1 protease inhibitors are substrates for the MDR1 multi-drug transporter. Biochemistry (Mosc) 1998;37:3594–3601.

32. Welcker M, Singer J, Loeb KR, et al. Multisite phosphorylation by Cdk2 and GSK3 controls cyclin E degradation. Mol Cell 2003;12:381–392. [PubMed: 14536078]

33. Strange R, Metcalfe T, Thackray L, Dang M. Apoptosis in normal and neoplastic mammary gland development. Microsc Res Tech 2001;52:171–181. [PubMed: 11169865]

34. Bartucci M, Morelli C, Mauro L, Ando S, Surmacz E. Differential insulin-like growth factor I receptor signaling and function in estrogen receptor (ER)-positive MCF-7 and ER-negative MDA-MB-231 breast cancer cells. Cancer Res 2001;61:6747–6754. [PubMed: 11559546]

35. Solit DB, Basso AD, Olshen AB, Scher HI, Rosen N. Inhibition of heat shock protein 90 function down-regulates Akt kinase and sensitizes tumors to Taxol. Cancer Res 2003;63:2139–2144. [PubMed: 12727831]

36. Yan J, Roy S, Apolloni A, Lane A, Hancock JF. Ras isoforms vary in their ability to activate Raf-1 and phosphoinositide 3-kinase. J Biol Chem 1998;273:24052–24056. [PubMed: 9727023]

37. Lev DC, Kim LS, Melnikova V, Ruiz M, Ananthaswamy HN, Price JE. Dual blockade of EGFR and ERK1/2 phosphorylation potentiates growth inhibition of breast cancer cells. Br J Cancer 2004;91:795–802. [PubMed: 15280923]

38. Gatti G, Di Biagio A, Casazza R, et al. The relationship between ritonavir plasma levels and side-effects: implications for therapeutic drug monitoring. AIDS 1999;13:2083–2089. [PubMed: 10546861]

39. Srethapakdi M, Liu F, Tavorath R, Rosen N. Inhibition of Hsp90 function by ansamycins causes retinoblastoma gene product-dependent G_1 arrest. Cancer Res 2000;60:3940–3946. [PubMed: 10919672]

40. Basso AD, Solit DB, Chiosis G, Giri B, Tsichlis P, Rosen N. Akt forms an intracellular complex with heat shock protein 90 (Hsp90) and Cdc37 and is destabilized by inhibitors of Hsp90 function. J Biol Chem 2002;277:39858–39866. [PubMed: 12176997]

41. Chiosis G, Timaul MN, Lucas B, et al. A small molecule designed to bind to the adenine nucleotide pocket of Hsp90 causes Her2 degradation and the growth arrest and differentiation of breast cancer cells. Chem Biol 2001;8:289–299. [PubMed: 11306353]

42. Diehl JA, Zindy F, Sherr CJ. Inhibition of cyclin D_1 phosphorylation on threonine-286 prevents its rapid degradation via the ubiquitin-proteasome pathway. Genes Dev 1997;11:957–952. [PubMed: 9136925]

43. Prince T, Sun L, Matts RL. Cdk2: a genuine protein kinase client of hsp90 and cdc37. Biochemistry (Mosc) 2005;44:15287–15295.

44. Dai K, Kobayashi R, Beach D. Physical interaction of mammalian CDC37 with CDK4. J Biol Chem 1996;271:22030–22034. [PubMed: 8703009]

45. Stepanova L, Leng X, Parker SB, Harper JW. Mammalian p50Cdc37 is a protein kinase-targeting subunit of Hsp90 that binds and stabilizes Cdk4. Genes Dev 1996;10:1491–1502. [PubMed: 8666233]

46. Mahony D, Parry DA, Lees E. Active cdk6 complexes are predominantly nuclear and represent only a minority of the cdk6 in T cells. Oncogene 1998;16:603–611. [PubMed: 9482106]

47. Liang J, Zubovitz J, Petrocelli T, et al. PKB/Akt phosphorylates p27, impairs nuclear import of p27 and opposes p27-mediated G_1 arrest. Nat Med 2002;8:1153–1160. [PubMed: 12244302]

48. Shin I, Yakes FM, Rojo F, et al. PKB/Akt mediates cell-cycle progression by phosphorylation of p27 (Kip1) at threonine 157 and modulation of its cellular localization. Nat Med 2002;8:1145–1152. [PubMed: 12244301]

49. Tsai EM, Wang SC, Lee JN, Hung MC. Akt activation by estrogen in estrogen receptor-negative breast cancer cells. Cancer Res 2001;61:8390–8392. [PubMed: 11731414]

50. Stover T, Kester M. Liposomal delivery enhances short-chain ceramide-induced apoptosis of breast cancer cells. J Pharmacol ExpTher 2003;307:468–475.

51. Klippel A, Reinhard C, Kavanaugh WM, Apell G, Escobedo MA, Williams LT. Membrane localization of phosphatidylinositol 3-kinase is sufficient to activate multiple signal-transducing kinase pathways. Mol Cell Biol 1996;16:4117–4127. [PubMed: 8754810]

52. Andjelkovic M, Alessi DR, Meier R, et al. Role of translocation in the activation and function of protein kinase B. J Biol Chem 1997;272:31515–31524. [PubMed: 9395488]

53. Zhang X, Vik TA. Growth factor stimulation of hematopoietic cells leads to membrane translocation of AKT1 protein kinase. Leuk Res 1997;21:849–856. [PubMed: 9393600]

54. Zampieri L, Bianchi P, Ruff P, Arbuthnot P. Differential modulation by estradiol of P-glycoprotein drug resistance protein expression in cultured MCF7 and T47D breast cancer cells. Anticancer Res 2002;22:2253–2259. [PubMed: 12174911]

55. Zhang R, Luo D, Miao R, et al. Hsp90-Akt phosphorylates ASK1 and inhibits ASK1-mediated apoptosis. Oncogene 2005;24:3954–3963. [PubMed: 15782121]

56. Schulte TW, Akinaga S, Soga S, et al. Antibiotic radicicol binds to the N-terminal domain of Hsp90 and shares important biologic activities with geldanamycin. Cell Stress Chaperones 1998;3:100–108. [PubMed: 9672245]

57. Rutherford SL, Lindquist S. Hsp90 as a capacitor for morphological evolution. Nature 1998;396:336–342. [PubMed: 9845070]

58. Norton L. A Gompertzian model of human breast cancer growth. Cancer Res 1988;48:7067–7071. [PubMed: 3191483]

59. Norton L, Simon R. The Norton-Simon hypothesis revisited. Cancer Treat Rep 1986;70:163–169. [PubMed: 3510732]

60. Takimoto CH, Rowinsky EK. Dose-intense paclitaxel: deja vu all over again? J Clin Oncol 2003;21:2810–2814. [PubMed: 12807932]
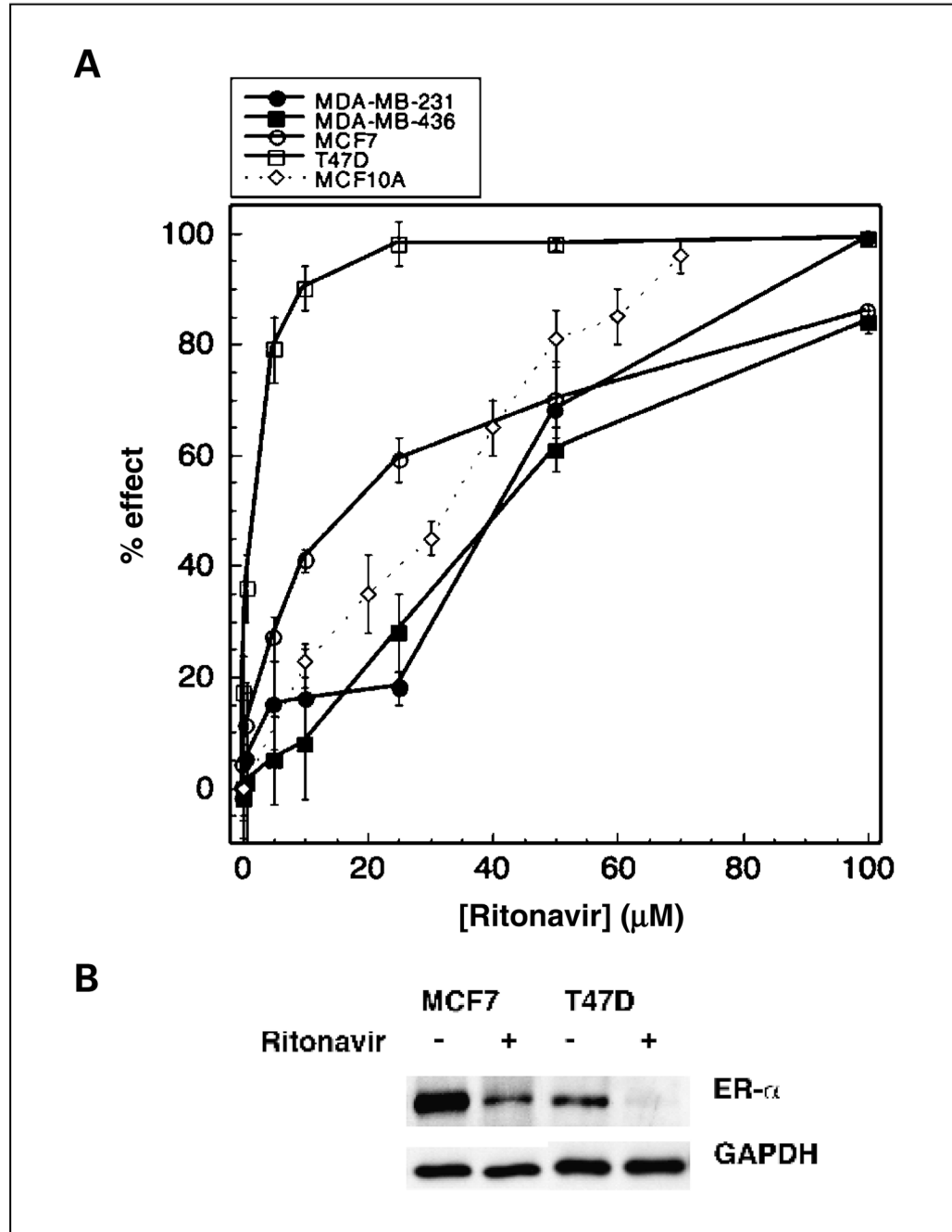
Fig. 1.
Ritonavir inhibits the proliferation of breast cancer lines and causes a reduction of ER-α. *A*,
ritonavir-mediated inhibition of growth ofT47D (□), MCF7 (○),MCF10A (◊), MDA-MB-436
(■), and MDA-MB-231 (●) cell lines was measured by MTTassay. Inhibition of cell growth
in the presence of ritonavir is expressed as a percentage of a vehicle control at 48 hours of
growth. *Points*, mean % inhibition; *bars*, SD. IC$_{50}$s were determined from the plot.
Representative of three experiments. *B*, ritonavir-mediated reduction of ER-α in the MCF7 and
T47D lines after 48-hour exposure to ritonavir was measured by Western blot as described in
Materials and Methods. Representative of three experiments. Protein measurements for each
lane were normalized to the lane's GAPDH control.
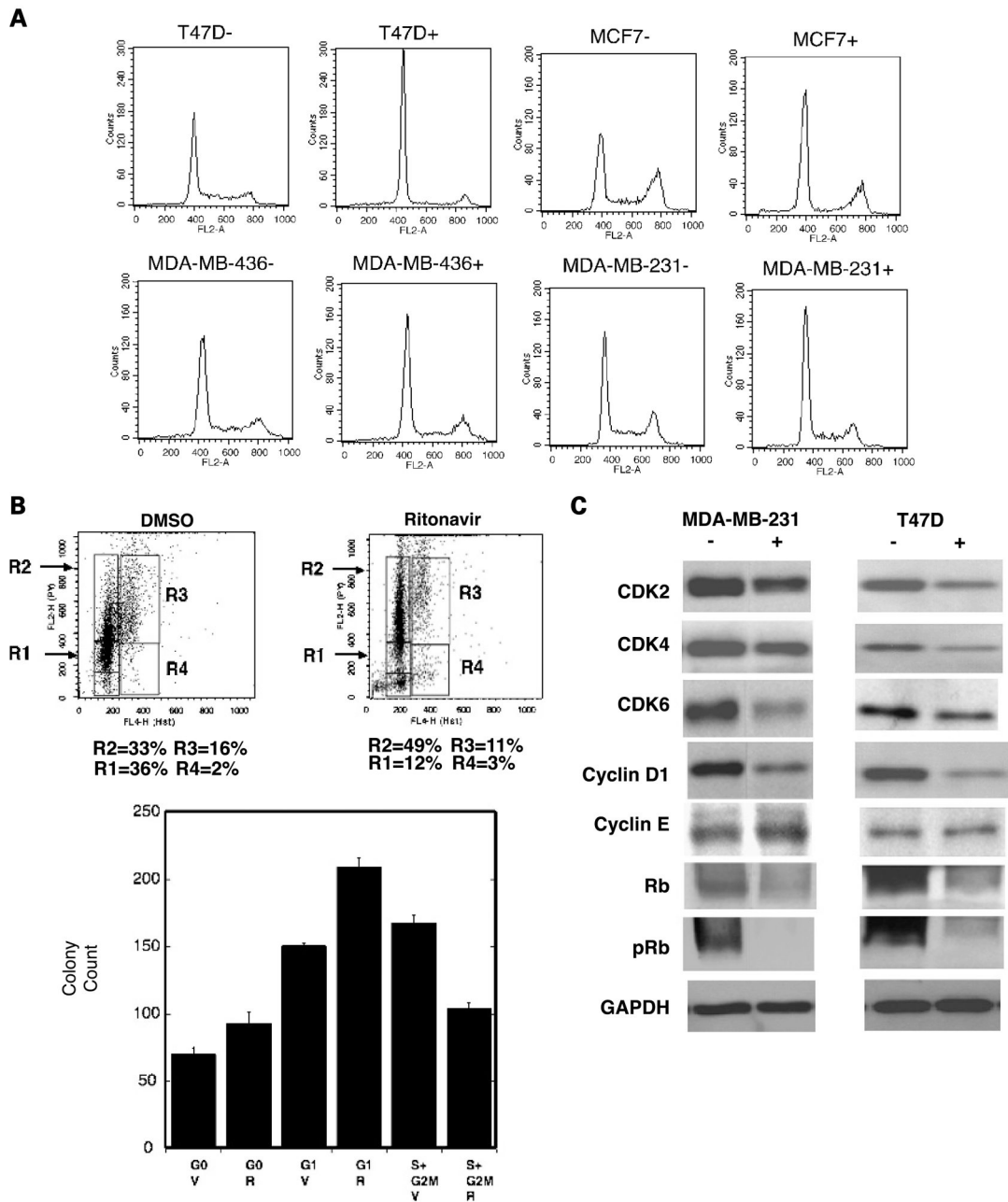
Fig. 2.
Ritonavir causes a G_1 arrest of $Rb^{+/+}$ breast cancer lines. *A*, flow cytometry analysis of PI staining of theT47D, MCF7, MDA-MB-436, and MDA-MB-231 lines at 48 hours of growth in the presence of DMSO vehicle (−) or ritonavir (+; 45 µmol/L). Representative of three experiments. Quantitation of PI flow cytometry is presented in Table 1. *B*, flow cytometry and clonogenic efficiency of sorted Hoechst/pyronin-stained MDA-MB-231cells.The cells were treated with ritonavir (IC_{50}, 45 µmol/L) for 24 hours and then prepared for flow cytometry as described in Materials and Methods. *Top*, Hoechst dye (*X axis*) and pyronin (*Y axis*) staining. *R1*, G_0; *R2*, G_1; *R3*, S+G_2−M; *R4*, sub-S + G_2−M. Percentage of total cells in the *R1* to *R4* boxes is indicated below the flow cytometry plot. *Bottom*, colony recovery from the G_0, G_1,

and S+ G_2-M regions. The plating experiments were done in triplicate, with 250 cells plated per condition, and the cells were grown for 21days in the absence of ritonavir, with medium changed every 3 days. On day 21, the plates were stained with crystal violet and colonies were counted. *V*, vehicle; *R*, ritonavir treatment of the cells before plating. *Bars*, SD. Differences were significant between paired V and R cell populations for each region of the cell cycle ($P < 0.05$). *C*, ritonavir depletes CDK, cyclin D_1, and pRb levels but not cyclin E in breast cancer lines. RIPA cell lysates were made from T47D or MDA-MB-231 lines treated for 24 hours with vehicle (−) or ritonavir (+) at the IC_{50} for proliferation (MDA-MB-231 = 45 µmol/L; T47D = 15 µmol/L). Lysate preparation and Western blot analysis were done as described in Materials and Methods. Quantitation of the Western blots is presented in Table 2. Protein measurements for each lane were normalized to the lane's GAPDH control.
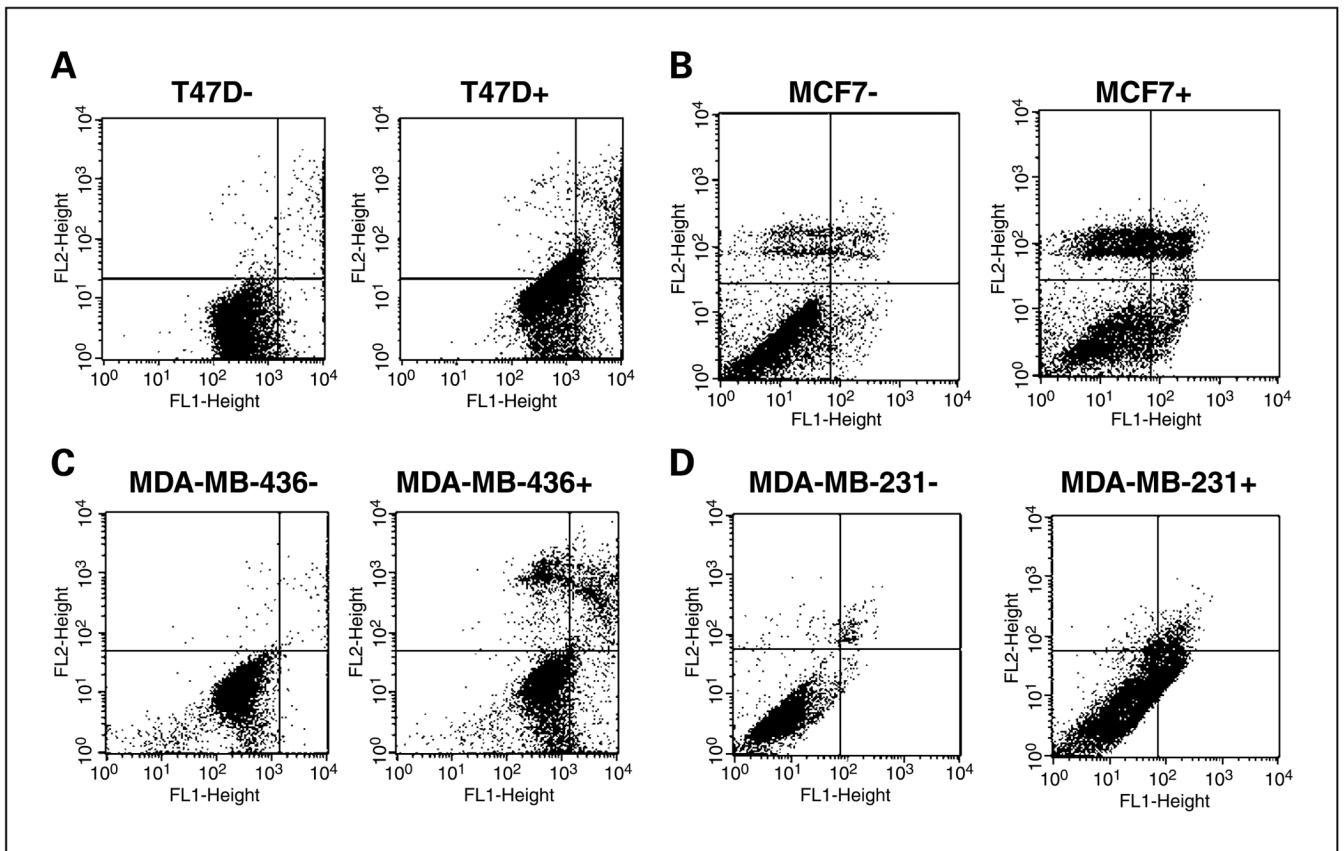
Fig. 3.
Ritonavir induces apoptosis in breast cancer lines. Flow cytometry of Annexin V-FITC (*X axis*)/PI (*Y axis*) staining of the (*A*) T47D, (*B*) MCF7, (*C*) MDA-MB-436 and (*D*) MDA-MB-231 lines at 48 hours of growth in the presence of vehicle (−) or ritonavir (+; 45 µmol/L). Quantitation of the quadrants of each plot is presented in Table 3.
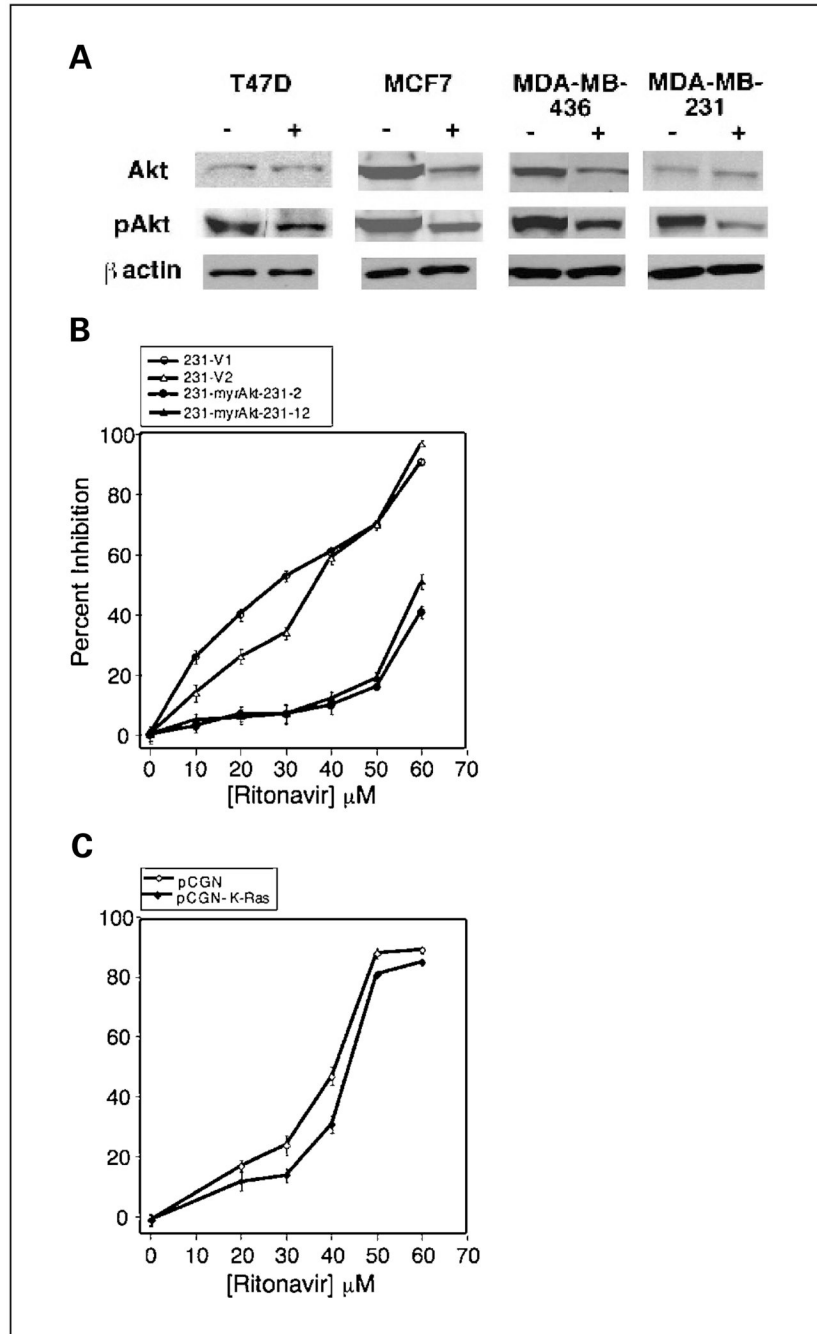
Fig. 4.
Ritonavir-induced inhibition of pAkt. *A*, ritonavir-treated breast cancer lines exhibit reduction of pAkt. RIPA cell lysates were made from T47D, MCF7, MDA-MB-436, and MDA-MB-231 lines treated for 24 hours with vehicle (−) or ritonavir (+) at the IC_{50} for proliferation. Western blot analysis was done as described in Materials and Methods and normalized to a β-actin control. Quantitation is presented in Table 4. *B*, stable overexpression of constitutively activated myristoyl-Akt increases the ritonavir IC_{50} of the MDA-MB-231 line. Two vector control lines (○ and Δ) are compared with two m-(Δ4-129)-Akt lines (● and ▲). *C*, stable overexpression of K-Ras V12 fails to significantly increase the ritonavir IC_{50} of the MDA-

MB-231 line. Results are derived from a vector clone (pCGN-V1) (◇) and pooled clonal lines stably transfected with K-RasV12 (pCGN-K-Ras) (♦).
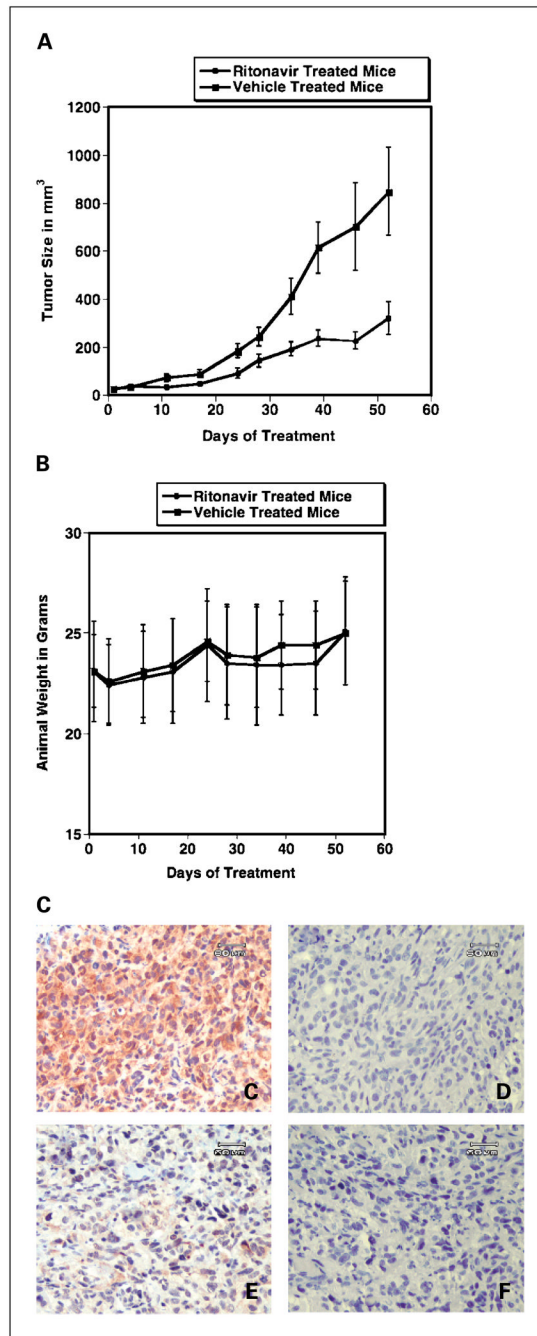
Fig. 5.
Ritonavir inhibits a murine breast cancer xenograft and down-regulates intratumoral Akt activity. *A*, tumor growth curve for ritonavir-treated (●) or vehicle-treated (■) mice bearing MDA-MB-231 tumors. The difference between the curves exhibited statistical significance. *Bars*, SE ($P < 0.001$ by Student's unpaired *t* test comparison of Gompertzian curve fits). *B*, weights were stable during treatment and similar for the ritonavir-treated (●) and vehicle-treated (■) mice. *Points*, mean animal weights *Bars*, SE. Method: A mammary fat pad model was used to test the response of xenograft tumors to ritonavir. A total of 1×10^6 cells were injected in a surgically exposed right mammary fat pad under general anesthesia. Tumors were grown for 21 days before initiation of treatment. Mice were treated with 40 mg/kg/d ritonavir

($n = 13$) or vehicle ($n = 14$). *C* to *F*, Akt activity is depleted in the plasma membrane/cytoplasmic region of MDA-MB-231 tumor cells following ritonavir treatment. MDA-MB-231 tumors were resected on day 52 at the completion of the xenograft experiment in (*A*), 1 hour following ritonavir administration, and fixed in formalin. Micrograph images are of the paracortical region of the tumor containing tumor cells, confirmed by light microscopy and immunohistochemical analysis (data not shown). Immunohistochemical assay for Akt activity for vehicle (*C*) or ritonavir (*E*) xenograft treatment. Peptide competition using the Akt phosphorylation site phosphopeptide immunogen was done for the vehicle (*D*) and ritonavir (*F*) treatment conditions at 1:500 dilution (see Materials and Methods). The tumors of vehicle-treated mice exhibited a predominantly plasma membrane/cytoplasmic predominant pattern, whereas the tumors of ritonavir-treated mice exhibited a speckled nuclear predominant pattern. Reduction of Akt kinase activity was significant based on cell counts ($P < 0.0001$, Student's *t* test). The ritonavir-treated tumors exhibit increased frequency of condensed and fragmented nuclei revealed in the peptide competition controls. Bar, 60 µm.
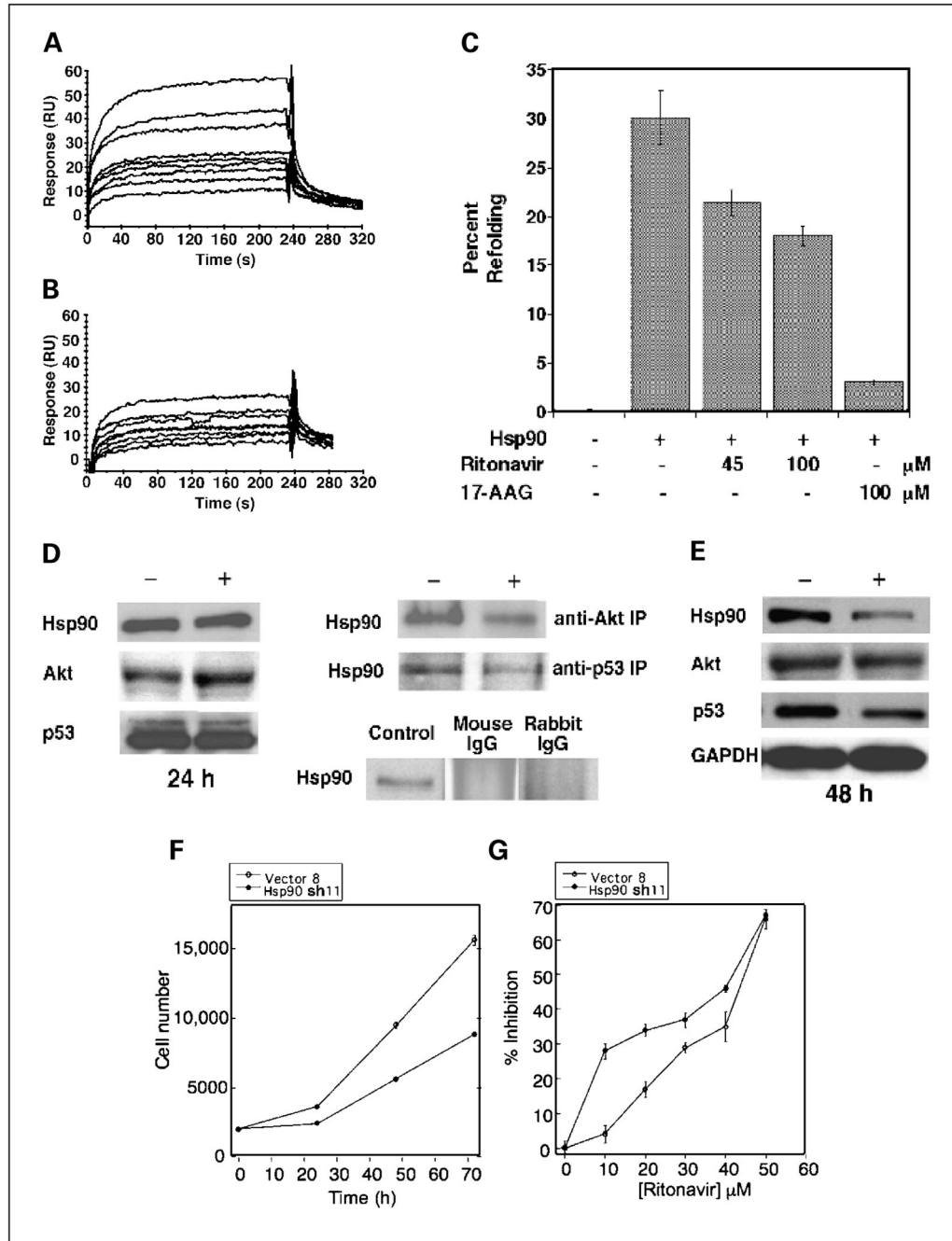
Fig. 6.
Ritonavir binds Hsp90, inhibits chaperone function and substrate association, depletes Hsp90 levels, and is potentiated by Hsp90α shRNA. *A*, surface plasmon resonance of ritonavir binding to purified HeLa cell Hsp90 attached to a Biacore CM5 sensor chip as described in Materials and Methods. Ritonavir was circulated in the flow cell at concentrations of 1, 4, 6, 8, 10, 12, 20, 25, and 37.5 µmol/L. Representative of three independent data sets. *B*, surface plasmon resonance of 17-AAG binding to purified HeLa cell Hsp90 attached to the same Biacore CM5 sensor chip as used in (*A*).The 17-AAG-positive control was circulated in the flow cell at concentrations of 0.6, 0.8, 3, 4, 5, 10, 20, and 35 µmol/L. Representative of three independent data sets. *C*, ritonavir inhibits ATP-dependent refolding of heat-treated luciferase. Heat-treated

luciferase was refolded and assayed by luminometry in the presence of ATP and an ATP-regenerating system. Addition of Hsp90 (11 µmol/L), ritonavir, and/or17-AAG was done as indicated. Refolding was dependent on Hsp90 and ATP and significantly reduced relative to the Hsp90-positive control (*column 2*), with addition of ritonavir (45 or 100 µmol/L) or 17-AAG (100 µmol/L). *Bars*, SD ($P < 0.05$, Student's *t* test for all comparisons with the Hsp90-positive control). *D*, ritonavir inhibits interaction of Hsp90 with Akt and mutant p53. *Left*, Hsp90, Akt, and mutant p53 levels are unaffected by ritonavir at 24 hours of treatment at the ritonavir IC_{50}. MDA-MB-231 cells were treated with DMSO vehicle (−) or at the ritonavir IC_{50} (+) for 24 hours, and RIPA lysates were probed by Western blotting with antisera to Hsp90, Akt, or mutant p53. Experiments were done in triplicate. A GAPDH control for normalization of Western blots is not shown. *Top right*, ritonavir inhibits immunoprecipitation of associated Hsp90 by an anti-Akt or anti-p53 antibody. MDA-MB-231 cell extracts from cells treated with vehicle (−) or ritonavir (+) at the IC_{50} were subject to immunoprecipitation by an anti-Akt or anti-p53 antibody (see Materials and Methods) followed by Western blot analysis by a Hsp90 antibody. Equal proteinwas used for the ritonavir and vehicle immunoprecipitations. Representative of three independent experiments. *Bottom right*, rabbit nonimmune IgG and murine nonimmune IgG control antibodies did not immunoprecipitate Hsp90 from RIPA lysates of untreated MDA-MB-231 cells. A Hsp90-positive control to indicate the mobility of Hp90 is shown from the same blot. *E*, ritonavir treatment for 48 hours depletes Hsp90 and p53 but not Akt. MDA-MB-231 cells were treated with DMSO vehicle (−) or at the ritonavir IC_{50} (+) for 48 hours, and RIPA lysates were probed by Western blotting in triplicate. GAPDH values were used to normalize the Western blot quantitation. *F*, the MDA-MB-231 line is dependent on Hsp90 for proliferation. The sh11 line expressing Hsp90α shRNA (●) exhibits significantly slower proliferation by MTTassay compared with the vector control lineV8 (○). *Points*, mean of octuplicate measurements; *bars*, SE. *G*, RNA interference targeting Hsp90 causes decreased resistance to ritonavir at low ritonavir concentrations. The sh11 (●) or vector control lineV8 (○) were exposed to varying concentrations of ritonavir for 48 hours and proliferation was measured by MTTassay. *Points*, mean of octuplicate measurements; *bars*, SE.

Table 1

Quantitation of ritonavir-induced G_0–G_1 arrest in breast cancer lines

Line	DMSO			Ritonavir (30 μmol/L)			Ritonavir (45 μmol/L)		
	G_0–G_1	S	G_2-M	G_0–G_1	S	G_2-M	G_0–G_1	S	G_2-M
T47D	53	6	40	73	17	10	84	8	7
MCF7	54	32	14	60	26	15	81	7	12
MDA-MB-436	60	27	13	61	25	14	65	19	16
MDA-MB-231	47	35	17	52	34	14	62	25	12

NOTE: Flow cytometry quantitation of G_0–G_1 arrest in breast cancer lines determined by analysis of PI-stained cells at 48 hours of ritonavir exposure. Profiling of PI incorporation was done by FACS can analysis using ModFit software. Results are representative of two or three replicate experiments.

Table 2

Quantitation of ritonavir-induced down-regulation of cyclin D_1 and CDK levels and inhibition of Rb phosphorylation in breast cancer lines

	MDA-MB-231			T47D	
	Fraction of control	**P**		**Fraction of control**	**P**
CDK2	0.64	0.05		0.81	0.002[*]
CDK4	0.59	0.02[*]		0.83	0.01[*]
CDK6	0.55	0.03[*]		0.70	0.02[*]
Cyclin D_1	0.39	0.0005[*]		0.62	0.002[*]
Cyclin E	0.96	0.98		0.98	0.82
Rb	0.91	0.07		0.31	0.0009[*]
pRb	0.30	0.0001[*]		0.25	0.0007[*]

NOTE: Triplicate measurements were made by Western blot at 24 hours of vehicle or ritonavir exposure at the proliferation IC_{50}. In all lines, GAPDH levels were unaffected by ritonavir.

[*]$P < 0.05$.

Table 3

Quantitation of ritonavir-induced apoptosis in breast cancer lines

Line	µmol/L	LL (%)	LR (%)	UR (%)	UL (%)
T47D	0	92	5	2	0.9
	45	57	18	11	14
MCF7	0	86	3	4	8
	45	53	8	14	25
MDA-MB-436	0	98	0.7	0.7	0.4
	45	63	19	9	9
MDA-MB-231	0	97	0.5	2	0.7
	45	77	16	6	2

NOTE: Flow cytometry was done and quantitated with CellQuest software. Cells were plated at 30% to 40% confluence, grown for 24 hours, and then treated with DMSO vehicle or ritonavir (45 µmol/ L) for an additional 48 hours. Results are representative of three experiments.

Abbreviations: L, bottom for the first letter; U, top for the first letter; L, left quadrant for the second letter; R, right quadrant for the second letter; LL, viable cells; LR, early apoptotic; UR, late apoptotic.

Table 4

Quantitation of ritonavir-induced inhibition of pAkt in breast cancer lines

	T47D	MCF7	Fraction of control at ritonavir IC$_{50}$ MDA-MB-436	MDA-MB-231
Akt	1.01	0.57 *	0.57 *	1.1
pAkt	0.49 *	0.61 *	0.56 *	0.60 *

NOTE: Triplicate measurements were made by Western blot at 24 hours of vehicle or ritonavir exposure at the proliferation IC$_{50}$. Fraction of control protein level in ritonavir-treated cells is shown. In all lines, β-actin levels were unaffected by ritonavir.

*
$P < 0.05$.